EMIC-Wave Driven Electron Precipitation observed by CALET on the International Space Station

A. Bruno[1,2], L. W. Blum[3], G. A. de Nolfo[1], R. Kataoka[4,5], S. Torii[6], A. D. Greeley[1,2], S. G. Kanekal[1], A. W. Ficklin[7], T. G. Guzik[7]and S. Nakahira[8]

[1]Heliophysics Science Division, NASA Goddard Space Flight Center, Greenbelt, MD, USA
[2]Department of Physics, Catholic University of America, Washington, DC, USA
[3]University of Colorado, Boulder, CO, USA
[4]National Institute of Polar Research, Tachikawa, Japan
[5]Department of Polar Science, SOKENDAI, Tachikawa, Japan
[6]Waseda Research Institute for Science and Engineering, Waseda University, Shinjuku, Japan
[7]Department of Physics and Astronomy, Louisiana State University, Baton Rouge, LA, USA
[8]Institute of Space and Astronautical Science, Japan Aerospace Exploration Agency, Sagamihara, Japan

Key Points:

- We present a study of relativistic electron precipitation into the atmosphere with CALET on the ISS during a radiation belt depletion event
- The magnetically conjugate measurements with the Van Allen Probes show that the observed precipitation was driven by dusk-side EMIC waves
- Combined wave and particle data suggest that the radiation belt flux dropout was caused by both wave scattering and outward losses

Corresponding author: Alessandro Bruno, `alessandro.bruno-1@nasa.gov`

Abstract

We present an analysis of the relativistic electron precipitation (REP) event measured by the CALorimetric Electron Telescope (CALET) experiment on board the International Space Station during a relatively weak geomagnetic storm on 31 December 2016. CALET observations were compared with the measurements of the Van Allen Probes in the near-equatorial plane to investigate the global radiation belt dynamics and the REP drivers. The magnetically conjugate observations from these two missions demonstrate that the significant MeV precipitation directly detected by CALET in low-Earth orbit during a period of radiation belt depletion following the passage of a high-speed stream, was associated with dusk-side electromagnetic ion cyclotron (EMIC) waves. In addition, the combined wave, REP and trapped electron data suggest that the reported radiation belt depletion can be likely ascribed to the concomitant loss effects of EMIC wave scattering driving the atmospheric precipitation, as well as outward radial diffusion associated with magnetopause shadowing.

Plain Language Summary

Relativistic electron precipitation (REP) is a space-weather phenomenon commonly observed at high latitudes, in which energetic electrons trapped in the geomagnetic field are lost into the Earth's atmosphere. Along with outward radial diffusion associated with magnetopause shadowing, it represents the primary loss mechanism for the outer radiation belt. While previous studies have demonstrated that REP can be caused by scattering with electromagnetic ion cyclotron (EMIC) waves, a direct contribution of this process to belt depletion events is still debated. In this work we examine a dropout event that occurred on 31 December 2016, comparing the REP observations of the CALorimetric Electron Telescope (CALET) on the International Space Station, with the magnetically conjugate wave measurements of the Van Allen Probes in the near-equatorial plane. The analysis of combined data demonstrates that the REP event detected by CALET was likely driven by EMIC waves, and that the observed radiation belt depletion can be attributed to the concomitant loss effects of EMIC wave scattering and magnetopause shadowing.

1 Introduction

The physical mechanisms controlling the acceleration and loss of trapped relativistic electrons in the radiation belts are complex, and there are a number of competing processes that can combine to produce net enhancements or depletions of the belts (e.g., Kanekal and Miyoshi (2021)). In particular, rapid flux dropouts are typically reported during the main phase of geomagnetic storms, and often observed simultaneously across the entire outer radiation belt, spanning all McIlwain's L-shells and occurring on timescales $<$ hours (Baker et al., 1994). While part of the contribution to the belt depletion can be attributed to adiabatic or disturbance storm-time (Dst) effects (e.g., X. Li et al. (1997); Kim and Chan (1997)), phase space density (PSD) measurements have shown that some of the loss is real (e.g., Turner et al. (2012)). While radiation belt diffusion models can now reproduce observed acceleration events quite accurately (e.g., Thorne et al. (2013)), radiation belt depletion events are often less well-captured (e.g., Tu et al. (2014); Drozdov et al. (2015)).

The two primary loss mechanisms for outer radiation belt electrons are magnetopause shadowing (e.g., Ukhorskiy et al. (2006); Tu et al. (2019)) and precipitation into Earth's atmosphere (e.g., Millan et al. (2007); Blum et al. (2013); Xiang et al. (2016)). Magnetopause losses, particularly in conjunction with outward radial diffusion, have been shown to contribute significantly to these dropouts (e.g., Shprits et al. (2006); Loto'aniu et al. (2010); Turner et al. (2012)). However, these processes are frequently unable to fully account for the full extent of observed depletions (e.g., Hudson et al. (2014); Turner et al.

(2014); Ozeke et al. (2017)). Often artificial "fast scattering" must be added to simulations to better match trapped particle measurements (e.g., Ozeke et al. (2017)), particularly to reproduce depletions at relatively low ($\lesssim$4) L-shells. Magnetopause losses are also inconsistent with some storm-time proton observations, which do not show similar dropouts as electrons (e.g., Borovsky et al. (2016); Hartley et al. (2013)).

Analysis of PSD evolution of energetic electrons in the inner magnetosphere has suggested that radiation belt depletions, particularly at relatively low pitch angles and high energies (>1 MeV), are consistent with scattering by electromagnetic ion cyclotron (EMIC) waves (e.g., Drozdov et al. (2019); Xiang et al. (2017, 2018)). In a statistical study of dropout events, Xiang et al. (2018) attributed losses at low (<4.5) Roederer's L^* regions to EMIC wave scattering, while those at larger L^* were attributed to a combination of magnetopause shadowing and EMIC wave scattering. However, while numerous studies have recently demonstrated that relativistic electron precipitation (REP) can be driven by EMIC waves (e.g., Z. Li et al. (2014); Blum et al. (2015); Capannolo et al. (2019)), the direct contribution of this process to radiation belt depletion events remains unconfirmed or elusive.

In this work we examine a radiation belt dropout event that occurred on 31 December 2016, during a period of relatively weak geomagnetic activity. During this time, NASA's Van Allen Probes (VAPs) were orbiting near the equatorial plane measuring both the trapped radiation belt population as well as plasma wave activity, while the CALorimetric Electron Telescope (CALET) on board the International Space Station (ISS) detected strong MeV electron precipitation. Using magnetically conjugate observations from these two platforms, here we investigate the evolution of the trapped as well as precipitating energetic electron population and the electromagnetic waves that contribute to these radiation belt dynamics.

2 Observations

CALET is a high-energy astroparticle physics experiment developed and operated by Japan in collaboration with Italy and USA (Torii, 2016). Installed on the Kibo module-exposed facility on the ISS in August 2015, it has been collecting data since October 2015 (Asaoka et al., 2019). The mission primary scientific goal is focused on investigations of cosmic-ray acceleration and transport processes through precise spectral measurement of the different particle populations – electrons, gamma-rays, protons, helium and heavier nuclei spectra – in a wide energy range from ∼1 GeV up to 1 PeV. Concomitant observational objectives include the study of solar modulation effects and the monitoring of the low-Earth orbit (LEO) radiation environment. In particular, constrained by the ISS orbit (∼400 km altitude and ∼51 deg inclination), CALET is able to detect high-energy solar particle events at relatively high geomagnetic latitudes, inner Van Allen belt protons in the South-Atlantic anomaly, and REP events near the inner boundary of the outer belt (Kataoka et al., 2016, 2020; Bruno et al., 2019, 2021; Ueno et al., 2020).

The CALET instrument is made up of three main components: a charge detector (CHD), a pre-shower imaging calorimeter (IMC) and a total absorption calorimeter (TASC) (Asaoka et al., 2018). Specifically, the REP analysis presented in this work is based on the count-rate information from the two orthogonal layers of plastic scintillators (CHDX and CHDY) constituting the CHD, placed at the top of the apparatus, with a detection threshold corresponding to ∼1.5 and ∼3.4 MeV electrons, respectively. REP intervals are recognizable as spikes in the CHD count-rate temporal profiles, and can be identified by requiring a count-rate ratio:

$$R_{xy} = N_X/N_Y > 1 + 3\,\sigma_{R_{xy}}, \tag{1}$$

N_X and N_Y being the CHDX and CHDY count rates, respectively, and $\sigma_{R_{xy}}$ the statistical uncertainty on R_{xy}. The count-rate ratio can be used to provide an estimate of the

event energy spectrum hardness. The magnetic local time (MLT) and the McIlwain's L parameters associated with ISS orbit were computed by using the 13^{th} generation International Geomagnetic Reference Field (Alken et al., 2021) and the Tsyganenko and Sitnov (2005) models for the description of the internal and external geomagnetic field, respectively.

In addition to data from CALET, we utilized particle and wave measurements from the VAPs (Mauk et al., 2013). In particular, the Magnetic Electron Ion Spectrometer (MagEIS) and the Relativistic Electron Proton Telescope (REPT) data were used to evaluated the outer-belt electron intensities (Baker et al., 2013; Blake et al., 2013). The magnetic-field measurements from the Electric and Magnetic Field Instrument Suite Integrated Science (EMFISIS; Kletzing et al. (2013)) were analyzed to investigate wave drivers. Finally, we took advantage of the electron observations from the Radiation Belt Monitor (RBM) of the MAXI instrument on board the Kibo module (Matsuoka et al., 2009) to infer the flux angular distribution at the ISS altitudes.

3 The 31 December 2016 dropout event

Figure 1 displays the time profiles of electron, interplanetary and geomagnetic data between 29 December 2016 and 3 January 2017. The top panel reports the CHD count rates (a), with CHDX and CHDY data indicated in red and blue, respectively. Panel b) shows the spin-averaged electron intensities (color code) measured by the REPT instrument as a function of L, at an energy (1.8 MeV) close to the CHDX threshold; for comparison, the black points denote the CHD observations based on the corresponding L-shell values. The next three panels (c, d, e) demonstrate the profiles of the 1-min resolution solar-wind speed and density and the z-component of the interplanetary magnetic field, based on the Deep Space Climate Observatory (DSCOVR) data time-shifted to the nose of the Earth's bow shock (`http://omniweb.gsfc.nasa.gov/`). Panels f) and g) display the variations of the Dst and the Auroral Electrojet (AE) indices, estimated with an 1-hour and an 1-min resolution, respectively. Finally, panel h) shows the magnetopause standoff distance (R_{MP}) based on the empirical model by Shue et al. (1998).

The initial few days of this period were characterized by enhanced outer-belt electron intensities and moderate geomagnetic activity, with a gradual decrease of the solar-wind speed down to ∼300 km/s. In this interval CALET detected a few REP events associated with substorm occurrence, along with a persistent background component at L∼3. The solar-wind parameters on 31 December indicate the passage of a co-rotating interaction region (CIR), followed by a high-speed stream (HSS) from an equatorial coronal hole. Within the CIR, the arrival of a stream interface is identified by the increasing speed and decreasing density at ∼12UT, as marked by the dashed vertical line. The preceding particle density enhancement at 10–12UT, up to values ∼65 cm^{-3}, is associated with the heliospheric plasma sheet, with multiple crossings of the heliospheric current sheet. The co-rotating HSS caused a strong compression of the Earth's magnetopause (see bottom panel), a rapid decrease of the outer-belt electron intensities, as demonstrated by the REPT measurements, along with a relatively weak geomagnetic activity (Dst$_{min}$=-29 nT). In addition, the belt dropout was accompanied by significant MeV precipitation detected by CALET in LEO.

The first enhancement in the CHD count rates was registered around 12UT in the pre-midnight sector, in correlation with the increased AE activity, and persisted for several hours. In particular, for two REP intervals around 12:15UT and 13:50UT, the ISS was found to be in close magnetic conjunction with the VAP-A and -B, respectively, enabling the investigation of possible wave drivers. The relative locations of the spacecraft in MLT and L-shell during these two periods are shown in the top panels of Figure 2. The color code indicates the CHDX count rates, while the black curves are the VAP-A (left) and -B (right) orbits during the two-hour intervals around the CALET REP ob-

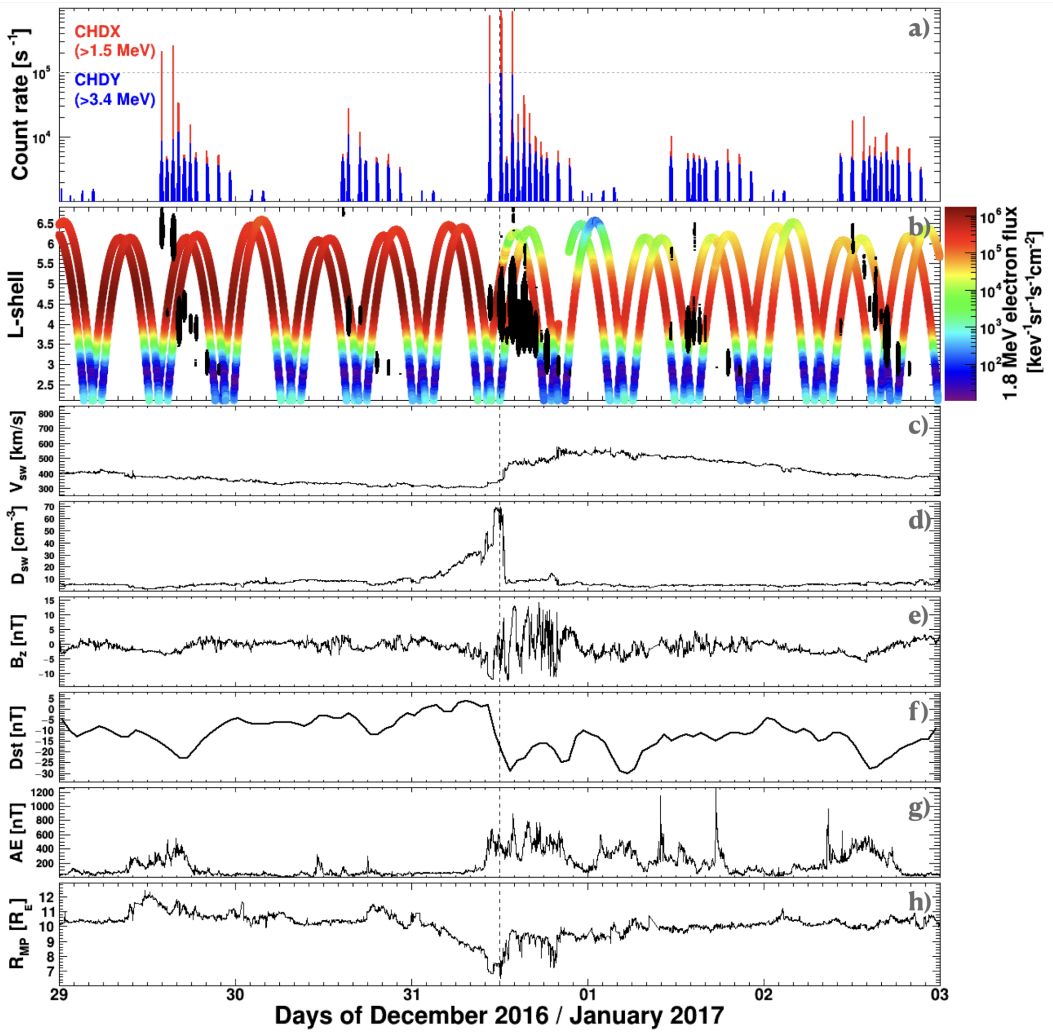

Figure 1. Time profile of electron, interplanetary and geomagnetic data between 29 December 2016 and 3 January 2017. From top to bottom: CHDX and CHDY count rates (a); 1.8 MeV electron intensity (color code) measured by the REPT instrument (b); solar-wind velocity (c) and density (d); interplanetary magnetic field z-component (e); Dst (f) and AE (g) indices; the magnetopause standoff distance (h). The dashed vertical line marks the arrival of a HSS at ∼12UT on December 31.

servations, with the thicker segments corresponding to the CALET precipitation detection intervals, as marked by dashed boxes in panel (d).

Magnetic field spectrograms from the EMFISIS instrument are presented in panels (b) and (c), showing wave activity in the kHz and Hz frequency ranges, respectively. The three white curves in the $b_{1,2}$ panels represent the electron cyclotron frequency multiplied by 0.1, 0.5 and 1.0; the white curves in the $c_{1,2}$ panels correspond – from top to bottom – to the proton, helium and oxygen gyro-frequencies. Hiss wave activity was observed close to Earth by both spacecraft, while chorus waves were measured by VAP-B at larger L-shells. Strong EMIC wave activity primarily in the He^+ frequency band was present during the transition from high- to low-density regions and observed by both spacecraft ∼90 min apart.

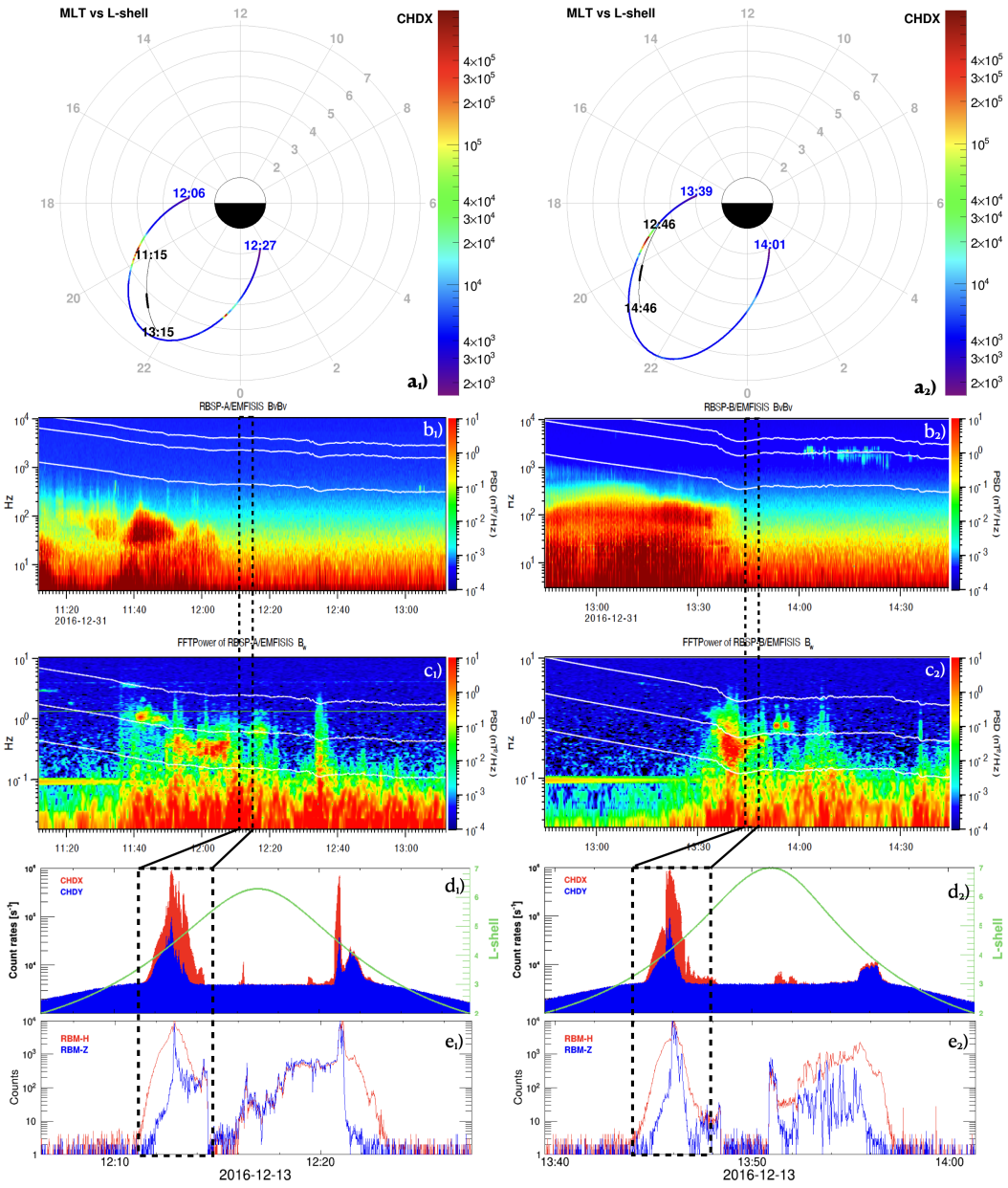

Figure 2. Electron and wave observations during the two selected intervals around 12:15UT (left panels) and 13:50UT (right panels). Panels $a_{1,2}$: orbit of the ISS as a function of McIlwain's L and MLT. The color code indicates the corresponding CHDX count rates. For comparison, the two black curves denote the VAP-A (left) and -B (right) orbits during the two-hour intervals around CALET detection times, corresponding to the thicker orbit segments. Panels $b_{1,2}$ and $c_{1,2}$: corresponding magnetic field spectral density measured by the EMFISIS instrument on board VAP-A (left) and -B (right), respectively, in the kHz ($b_{1,2}$) and Hz ($c_{1,2}$) frequency ranges. Panels $d_{1,2}$: time profiles of the count rates ($d_{1,2}$) measured by CHDX and CHDY, with the green curves denoting the L values along the ISS orbit. Panels $e_{1,2}$: MAXI/RBM count temporal profile.

The corresponding temporal profiles of the CHDX and CHDY count rates during these two consecutive orbits are shown in panel (d). The green curves denote the McIl-

wain's L values along the ISS orbit. For both intervals, the CHD count rates were found to peak mostly around specific L-shells centered at ∼4.5 and ∼4.2 for the first and the second orbit, respectively. Highly structured strong precipitation is observed on both orbits, in close magnetic conjunction and coincident in time with the EMIC wave activity observed by VAP-A and -B.

Finally, panel (e) displays the >0.3 MeV electron counts measured by the RBM detector, which consists of two identical orthogonal sensors, RBM-H and RBM-Z, pointing to the horizontal and vertical (zenith) directions, thus corresponding to relatively high and low pitch-angle values, respectively, Consequently, while both CALET and RBM data include both quasi-trapped and precipitating electron components, the comparison between RBM-H and RBM-Z provides information about the local pitch angle distribution. While at slightly lower energies, RBM observations confirm the detected electron fluxes are isotropic during the CHD enhancements, consistent with the presence of a significant contribution of bounce loss-cone electrons as expected during REP events.

4 Discussion

The results presented in Figures 1 and 2 reveal REP activity occurring during a CIR/HSS-driven event, with two of the REP intervals in close magnetic conjunction to EMIC wave activity near the magnetic equator. The EMIC waves and precipitation occurred in a relatively localized radial extent, consistent with past observations (e.g., Zhang et al. (2014); Blum et al. (2015, 2017); Capannolo et al. (2021)). Precipitation detected by CALET in the same dusk sector on consecutive orbits, along with EMIC wave activity observed in the same region first by VAP-A at ∼12:10UT and then by VAP-B at ∼13:45UT suggests this wave activity and the precipitation it drove persisted for at least ∼1.5 hours.

To better understand how this precipitation contributed to the overall dynamics of the trapped electron population, we examined the PSD evolution of the radiation belt during this period. Figure 3 presents radial PSD profiles from VAP-A (left) and -B (right) for a 0.11 $G^{0.5}R_E$ value of the second adiabatic invariant (K) and three different values of the first adiabatic invariant (mu), 501, 1000, and 1995 MeV/G, as a function of the L^*; corresponding kinetic energy values are also reported on the X axis. Details of the PSD estimation can be found in Boyd et al. (2018). During this period, strong PSD loss was observed first after ∼9:30UT in the outer half of the belt, at $L^* \geq 4.5$. By the following inbound orbits after ∼16UT this depletion has spread throughout the entire outer radiation belt (L^*∼3.5–4 through 5.5).

In addition to the weak Dst signature during this event, Figure 3 indicates that significant real loss of MeV electrons (not simply due to adiabatic effects) occurred, as suggested by the decreasing PSD throughout the outer belt between ∼12-24UT on 31 December 2016. The magnetopause was compressed down to ∼6.6 R_E at 12UT, due to the enhanced proton density and solar-wind dynamic pressure associated with a HSS (see Figure 1). The radial PSD profiles show patterns similar to those often associated with outward loss to the magnetospause (e.g., Turner et al. (2012); Shprits et al. (2017)), likely occurring during this event as well. However, in this case, strong MeV precipitation into Earth's atmosphere was also occurring, as confirmed by the CALET observations at low altitude. This suggests that even during radiation belt depletion events that appear primarily due to outward losses, based on the analysis of PSD profiles and solar-wind parameters alone, wave-driven precipitation of relativistic electrons may occur concurrently, providing a significant contribution to the belt dynamics and the energy input to the Earth's atmosphere.

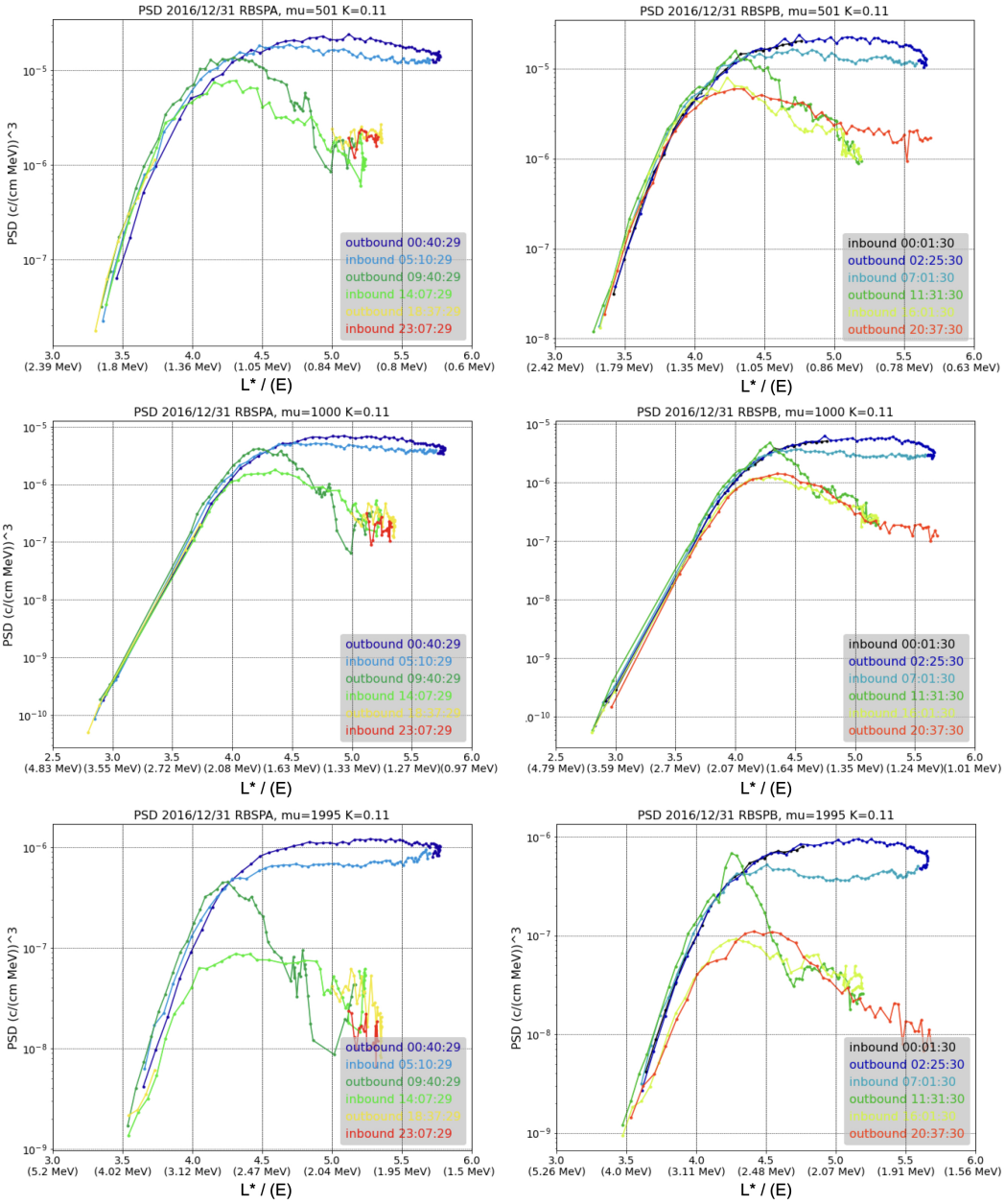

Figure 3. Radial PSD profiles from VAP-A (left) and -B (right) on December 31, 2016, for K=0.11 $G^{0.5}R_E$ and three different mu values: 501 (top), 1000 (middle) and 1995 (bottom) MeV/G, as a function of the L^*; corresponding kinetic energy values are also reported in brackets on the X axis.

5 Summary and Conclusions

We presented a study of the REP event measured by the CALET experiment on board the ISS during the CIR/HSS-driven event on 31 December 2016. CALET observations have been compared with the electron and wave measurements of the VAPs in highly-eccentric orbit to investigate the REP drivers and the global radiation belt evolution. The combined wave, REP and trapped electron data suggest that both losses to the magnetopause as well as to the atmosphere may have occurred during this event, caus-

ing the reported depletion. In particular, the analysis of the radial PSD belt profiles indicates a dominant loss contribution likely due to outward radial diffusion associated with magnetopause shadowing. On the other hand, the magnetically conjugate observations from the two experiments demonstrate that a significant dusk-side EMIC wave activity was likely responsible for the strong MeV precipitation directly detected by CALET in LEO, providing evidence of a relevant contribution of EMIC wave-driven precipitation to the radiation belt dropout dynamics.

Open Research

The CALET/CHD data used in this analysis were provided by the Waseda CALET Operation Center at Waseda University, and are publicly available via DARTS at ISAS/JAXA (`https://data.darts.isas.jaxa.jp/pub/calet/cal-v1.1/CHD/level1.1/`). The MAXI/RBM data provided by RIKEN, JAXA and the MAXI team, via DARTS at ISAS/JAXA (`https://data.darts.isas.jaxa.jp/pub/maxi/rbm/`). VAP wave data were obtained from `https://space.physics.uiowa.edu/` via the data analysis system (das2); VAP-A and -B electron data were downloaded from `https://rbsp-ect.newmexicoconsortium.org/data_pub/rbspa/ECT/level2/` and `https://rbsp-ect.newmexicoconsortium.org/data_pub/rbspb/ECT/level2/`, respectively.

Acknowledgments

A.B. and L.W.B. acknowledge support from NASA/Living With a Star Science program NNH20ZDA001N-LWS and from Heliophysics Internal Scientist Funding Model (ISFM) grant HISFM21. A.W.F and T.G.G. acknowledge support from NASA/CALET award 80NSSC20K0397 at Louisiana State University.

References

Alken, P., Thébault, E., Beggan, C. D., Amit, H., Aubert, J., Baerenzung, J., ... Zhou, Z. Z. . B. (2021). International geomagnetic reference field: the thirteenth generation. *Earth Planet Sp*, *73*, 49. doi: 10.1186/s40623-020-01288-x

Asaoka, Y., Adriani, O., Akaike, Y., Asano, K., Bagliesi, M. G., Berti, E., ... Yoshida, K. (2019). The CALorimetric electron telescope (CALET) on the international space station: Results from the first two years on orbit. *Journal of Physics: Conference Series*, *1181*, 012003. doi: 10.1088/1742-6596/1181/1/012003

Asaoka, Y., Ozawa, S., Torii, S., Adriani, O., Akaike, Y., Asano, K., ... Yuda, T. (2018). On-orbit operations and offline data processing of calet onboard the iss. *Astroparticle Physics*, *100*, 29-37. doi: 10.1016/j.astropartphys.2018.02.010

Baker, D. N., Blake, J. B., Callis, L. B., Cummings, J. R., Hovestadt, D., Kanekal, S., ... Zwickl, R. D. (1994). Relativistic electron acceleration and decay time scales in the inner and outer radiation belts: Sampex. *Geophysical Research Letters*, *21*(6), 409-412. doi: 10.1029/93GL03532

Baker, D. N., Kanekal, S. G., Hoxie, V. C., Batiste, S., Bolton, M., Li, X., ... Friedel, H. E. S. . R. (2013). The relativistic electron-proton telescope (rept) instrument on board the radiation belt storm probes (rbsp) spacecraft: Characterization of Earth's radiation belt high-energy particle populations. *Space Sci Rev*, *179*, 337. doi: 10.1007/s11214-012-9950-9

Blake, J. B., Carranza, P. A., Claudepierre, S. G., Clemmons, J. H., Jr., W. R. C., Dotan, Y., ... Zakrzewski, M. P. (2013). The magnetic electron ion spectrometer (mageis) instruments aboard the radiation belt storm probes (rbsp) spacecraft. *Space Sci Rev*, *179*, 383. doi: 10.1007/s11214-013-9991-8

Blum, L. W., Bonnell, J. W., Agapitov, O., Paulson, K., & Kletzing, C. (2017).

EMIC wave scale size in the inner magnetosphere: Observations from the dual van allen probes. *Geophysical Research Letters*, *44*(3), 1227-1233. doi: 10.1002/2016GL072316

Blum, L. W., Halford, A., Millan, R., Bonnell, J. W., Goldstein, J., Usanova, M., ... Li, X. (2015). Observations of coincident EMIC wave activity and duskside energetic electron precipitation on 18–19 january 2013. *Geophysical Research Letters*, *42*(14), 5727-5735. doi: 10.1002/2015GL065245

Blum, L. W., Schiller, Q., Li, X., Millan, R., Halford, A., & Woodger, L. (2013). New conjunctive cubesat and balloon measurements to quantify rapid energetic electron precipitation. *Geophysical Research Letters*, *40*(22), 5833-5837. doi: 10.1002/2013GL058546

Borovsky, J. E., Cayton, T. E., Denton, M. H., Belian, R. D., Christensen, R. A., & Ingraham, J. C. (2016). The proton and electron radiation belts at geosynchronous orbit: Statistics and behavior during high-speed stream-driven storms. *Journal of Geophysical Research: Space Physics*, *121*(6), 5449-5488. doi: 10.1002/2016JA022520

Boyd, A. J., Turner, D. L., Reeves, G. D., Spence, H. E., Baker, D. N., & Blake, J. B. (2018). What causes radiation belt enhancements: A survey of the van allen probes era. *Geophysical Research Letters*, *45*(11), 5253-5259. doi: 10.1029/2018GL077699

Bruno, A., Blum, L., de Nolfo, G. A., Ficklin, A. W., & Guzik, T. G. (2021). Relativistic Electron Precipitation Observations with CALET on the International Space Station. In *Proceedings of 37th International Cosmic Ray Conference — PoS(ICRC2021)* (Vol. 395, p. 1295). doi: 10.22323/1.395.1295

Bruno, A., de Nolfo, G. A., Ficklin, A. W., Guzik, T. G., & Cannady, N. (2019). Space Weather Observations during September 2017 with CALET on the International Space Station. In *Proceedings of 36th International Cosmic Ray Conference — PoS(ICRC2019)* (Vol. 358, p. 1063). doi: 10.22323/1.358.1063

Capannolo, L., Li, W., Ma, Q., Shen, X.-C., Zhang, X.-J., Redmon, R. J., ... Raita, T. (2019). Energetic electron precipitation: Multievent analysis of its spatial extent during EMIC wave activity. *Journal of Geophysical Research: Space Physics*, *124*(4), 2466-2483. doi: 10.1029/2018JA026291

Capannolo, L., Li, W., Spence, H., Johnson, A. T., Shumko, M., Sample, J., & Klumpar, D. (2021). Energetic electron precipitation observed by firebird-ii potentially driven by EMIC waves: Location, extent, and energy range from a multievent analysis. *Geophysical Research Letters*, *48*(5), e2020GL091564. doi: 10.1029/2020GL091564

Drozdov, A. Y., Aseev, N., Effenberger, F., Turner, D. L., Saikin, A., & Shprits, Y. Y. (2019). Storm time depletions of multi-mev radiation belt electrons observed at different pitch angles. *Journal of Geophysical Research: Space Physics*. doi: 10.1029/2019JA027332

Drozdov, A. Y., Shprits, Y. Y., Orlova, K. G., Kellerman, A. C., Subbotin, D. A., Baker, D. N., ... Reeves, G. D. (2015). Energetic, relativistic, and ultrarelativistic electrons: Comparison of long-term verb code simulations with van allen probes measurements. *Journal of Geophysical Research: Space Physics*, *120*(5), 3574-3587. doi: 10.1002/2014JA020637

Hartley, D. P., Denton, M. H., Green, J. C., Onsager, T. G., Rodriguez, J. V., & Singer, H. J. (2013). Case studies of the impact of high-speed solar wind streams on the electron radiation belt at geosynchronous orbit: Flux, magnetic field, and phase space density. *Journal of Geophysical Research: Space Physics*, *118*(11), 6964-6979. doi: 10.1002/2013JA018923

Hudson, M. K., Baker, D. N., Goldstein, J., Kress, B. T., Paral, J., Toffoletto, F. R., & Wiltberger, M. (2014). Simulated magnetopause losses and van allen probe flux dropouts. *Geophysical Research Letters*, *41*(4), 1113-1118. doi: 10.1002/2014GL059222

Kanekal, S., & Miyoshi, Y. (2021). Dynamics of the terrestrial radiation belts: a review of recent results during the varsiti (variability of the sun and its terrestrial impact) era, 2014–2018. *Prog Earth Planet Sci*, *8*, 35. doi: 10.1186/s40645-021-00413-y

Kataoka, R., Asaoka, Y., Torii, S., Nakahira, S., Ueno, H., Miyake, S., ... Tanaka, Y. (2020). Plasma waves causing relativistic electron precipitation events at international space station: Lessons from conjunction observations with arase satellite. *Journal of Geophysical Research: Space Physics*, *125*(9), e2020JA027875. doi: 10.1029/2020JA027875

Kataoka, R., Asaoka, Y., Torii, S., Terasawa, T., Ozawa, S., Tamura, T., ... Mori, M. (2016). Relativistic electron precipitation at international space station: Space weather monitoring by calorimetric electron telescope. *Geophysical Research Letters*, *43*(9), 4119-4125. doi: 10.1002/2016GL068930

Kim, H.-J., & Chan, A. A. (1997). Fully adiabatic changes in storm time relativistic electron fluxes. *Journal of Geophysical Research: Space Physics*, *102*(A10), 22107-22116. doi: 10.1029/97JA01814

Kletzing, C. A., Kurth, W. S., Acuna, M., MacDowall, R. J., Torbert, R. B., Averkamp, T., ... Tyler, R. M. T. . J. (2013). The electric and magnetic field instrument suite and integrated science (emfisis) on rbsp. *Space Sci Rev*, *179*, 127. doi: 10.1007/s11214-013-9993-6

Li, X., Baker, D. N., Temerin, M., Cayton, T. E., Reeves, E. G. D., Christensen, R. A., ... Kanekal, S. G. (1997). Multisatellite observations of the outer zone electron variation during the november 3–4, 1993, magnetic storm. *Journal of Geophysical Research: Space Physics*, *102*(A7), 14123-14140. doi: 10.1029/97JA01101

Li, Z., Millan, R. M., Hudson, M. K., Woodger, L. A., Smith, D. M., Chen, Y., ... Spence, H. E. (2014). Investigation of EMIC wave scattering as the cause for the barrel 17 january 2013 relativistic electron precipitation event: A quantitative comparison of simulation with observations. *Geophysical Research Letters*, *41*(24), 8722-8729. doi: 10.1002/2014GL062273

Loto'aniu, T. M., Singer, H. J., Waters, C. L., Angelopoulos, V., Mann, I. R., Elkington, S. R., & Bonnell, J. W. (2010). Relativistic electron loss due to ultralow frequency waves and enhanced outward radial diffusion. *Journal of Geophysical Research: Space Physics*, *115*(A12), A12245. doi: 10.1029/2010JA015755

Matsuoka, M., Kawasaki, K., Ueno, S., Tomida, H., Kohama, M., Suzuki, M., ... Ebisawa, K. (2009, 10). The MAXI Mission on the ISS: Science and Instruments for Monitoring All-Sky X-Ray Images. *Publications of the Astronomical Society of Japan*, *61*(5), 999-1010. doi: 10.1093/pasj/61.5.999

Mauk, B. H., Fox, N. J., Kanekal, S. G., Kessel, R. L., Sibeck, D. G., & Ukhorskiy, A. (2013). Science objectives and rationale for the radiation belt storm probes mission. In N. Fox & J. L. Burch (Eds.), *The van allen probes mission* (pp. 3–27). Boston, MA: Springer US. doi: 10.1007/978-1-4899-7433-4_2

Millan, R. M., Lin, R. P., Smith, D. M., & McCarthy, M. P. (2007). Observation of relativistic electron precipitation during a rapid decrease of trapped relativistic electron flux. *Geophysical Research Letters*, *34*(10). doi: 10.1029/2006GL028653

Ozeke, L. G., Mann, I. R., Murphy, K. R., Sibeck, D. G., & Baker, D. N. (2017). Ultra-relativistic radiation belt extinction and ulf wave radial diffusion: Modeling the september 2014 extended dropout event. *Geophysical Research Letters*, *44*(6), 2624-2633. doi: 10.1002/2017GL072811

Shprits, Y. Y., Kellerman, A., Aseev, N., Drozdov, A. Y., & Michaelis, I. (2017). Multi-mev electron loss in the heart of the radiation belts. *Geophysical Research Letters*, *44*(3), 1204-1209. doi: 10.1002/2016GL072258

Shprits, Y. Y., Thorne, R. M., Friedel, R., Reeves, G. D., Fennell, J., Baker, D. N.,

& Kanekal, S. G. (2006). Outward radial diffusion driven by losses at magnetopause. *Journal of Geophysical Research: Space Physics*, *111*(A11). doi: 10.1029/2006JA011657

Shue, J.-H., Song, P., Russell, C. T., Steinberg, J. T., Chao, J. K., Zastenker, G., ... Kawano, H. (1998). Magnetopause location under extreme solar wind conditions. *Journal of Geophysical Research: Space Physics*, *103*(A8), 17691-17700. doi: 10.1029/98JA01103

Thorne, R. M., Li, W., Ni, B., Ma, Q., Bortnik, J., Chen, L., ... Claudepierre, S. G., S. G. & Kanekal (2013). Rapid local acceleration of relativistic radiation-belt electrons by magnetospheric chorus. *Nature*, *504*(5), 411-414. doi: 10.1038/nature12889

Torii, S. (2016). The CALorimetric Electron Telescope (CALET): a High-Energy Astroparticle Physics Observatory on the International Space Stati. In *Proceedings of the 34th International Cosmic Ray Conference — pos(icrc2015)* (Vol. 236, p. 581). doi: 10.22323/1.236.0581

Tsyganenko, N. A., & Sitnov, M. I. (2005). Modeling the dynamics of the inner magnetosphere during strong geomagnetic storms. *Journal of Geophysical Research: Space Physics*, *110*(A3). doi: 10.1029/2004JA010798

Tu, W., Cunningham, G. S., Chen, Y., Morley, S. K., Reeves, G. D., Blake, J. B., ... Spence, H. (2014). Event-specific chorus wave and electron seed population models in dream3d using the van allen probes. *Geophysical Research Letters*, *41*(5), 1359-1366. doi: 10.1002/2013GL058819

Tu, W., Xiang, Z., & Morley, S. K. (2019). Modeling the magnetopause shadowing loss during the june 2015 dropout event. *Geophysical Research Letters*, *46*(16), 9388-9396. doi: 10.1029/2019GL084419

Turner, D. L., Angelopoulos, V., Morley, S. K., Henderson, M. G., Reeves, G. D., Li, W., ... Rodriguez, J. V. (2014). On the cause and extent of outer radiation belt losses during the 30 september 2012 dropout event. *Journal of Geophysical Research: Space Physics*, *119*(3), 1530-1540. doi: 10.1002/2013JA019446

Turner, D. L., Shprits, Y., & Hartinger, V., M. & Angelopoulos. (2012). Explaining sudden losses of outer radiation belt electrons during geomagnetic storms. *Nature Phys*, *8*(5), 208-212. doi: 10.1038/nphys2185

Ueno, H., Nakahira, S., Kataoka, R., Asaoka, Y., Torii, S., Ozawa, S., ... Ricciarini, S. (2020). Radiation dose during relativistic electron precipitation events at the international space station. *Space Weather*, *18*(7), e2019SW002280. doi: 10.1029/2019SW002280

Ukhorskiy, A. Y., Anderson, B. J., Brandt, P. C., & Tsyganenko, N. A. (2006). Storm time evolution of the outer radiation belt: Transport and losses. *Journal of Geophysical Research: Space Physics*, *111*(A11). doi: 10.1029/2006JA011690

Xiang, Z., Ni, B., Zhou, C., Zou, Z., Gu, X., Zhao, Z., ... Reeves, G. (2016). Multi-satellite simultaneous observations of magnetopause and atmospheric losses of radiation belt electrons during an intense solar wind dynamic pressure pulse. *Annales Geophysicae*, *34*(5), 493–509. doi: 10.5194/angeo-34-493-2016

Xiang, Z., Tu, W., Li, X., Ni, B., Morley, S. K., & Baker, D. N. (2017). Understanding the mechanisms of radiation belt dropouts observed by van allen probes. *Journal of Geophysical Research: Space Physics*, *122*(10), 9858-9879. doi: 10.1002/2017JA024487

Xiang, Z., Tu, W., Ni, B., Henderson, M. G., & Cao, X. (2018). A statistical survey of radiation belt dropouts observed by van allen probes. *Geophysical Research Letters*, *45*(16), 8035-8043. doi: 10.1029/2018GL078907

Zhang, J.-C., Saikin, A. A., Kistler, L. M., Smith, C. W., Spence, H. E., Mouikis, C. G., ... Jordanova, V. K. (2014). Excitation of EMIC waves detected by the van allen probes on 28 april 2013. *Geophysical Research Letters*, *41*(12), 4101-4108. doi: 10.1002/2014GL060621